

Marquette University

e-Publications@Marquette

Mechanical Engineering Faculty Research and
Publications

Mechanical Engineering, Department of

1-2019

Effect of Diffusion Distance on Evolution of Kirkendall Pores in Titanium-Coated Nickel Wires

Aaron R. Yosta
Northwestern University

Dinc Erdeniz
Marquette University, dinc.erdeniz@marquette.edu

Ashley E. Paz y Puente
University of Cincinnati

David C. Dunanda
Northwestern University

Follow this and additional works at: https://epublications.marquette.edu/mechengin_fac



Part of the [Mechanical Engineering Commons](#)

Recommended Citation

Yosta, Aaron R.; Erdeniz, Dinc; Paz y Puente, Ashley E.; and Dunanda, David C., "Effect of Diffusion Distance on Evolution of Kirkendall Pores in Titanium-Coated Nickel Wires" (2019). *Mechanical Engineering Faculty Research and Publications*. 244.
https://epublications.marquette.edu/mechengin_fac/244

Marquette University

e-Publications@Marquette

Mechanical Engineering Faculty Research and Publications/College of Arts and Sciences

This paper is NOT THE PUBLISHED VERSION; but the author's final, peer-reviewed manuscript. The published version may be accessed by following the link in the citation below.

Intermetallics, Vol. 104 (January 2019): 124-132. [DOI](#). This article is © Elsevier and permission has been granted for this version to appear in [e-Publications@Marquette](#). Elsevier does not grant permission for this article to be further copied/distributed or hosted elsewhere without the express permission from Elsevier.

Effect of Diffusion Distance on Evolution of Kirkendall Pores in Titanium-Coated Nickel Wires

Aaron R. Yosta¹

Department of Materials Science and Engineering, Northwestern University, Evanston, IL

Dinc Erdeniz²

Department of Materials Science and Engineering, Northwestern University, Evanston, IL

Ashley E. Paz y Puente

Department of Mechanical and Materials Engineering, University of Cincinnati, Cincinnati, OH

David C. Dunanda

Department of Materials Science and Engineering, Northwestern University, Evanston, IL

Abstract

Microtubes of near-equiatomic nickel-titanium (NiTi) alloys can be created *via* the Kirkendall effect during Ni—Ti interdiffusion, when nickel wires are surface-coated with titanium *via* pack cementation and subsequently

homogenized. This study explores the effect of diffusion distance upon Kirkendall microtube formation in NiTi by considering a range of Ni wire diameters. For Ni wire diameters of 25, 50 and 100 μm , titanized at 925 $^{\circ}\text{C}$ for 0.5, 2, and 8 h to achieve average NiTi composition, partial interdiffusion occurs concurrently with Ti surface deposition, resulting in concentric shells of NiTi_2 , NiTi and Ni_3Ti around a Ni core, with some Kirkendall porosity created within the wires. Upon subsequent homogenization at 925 $^{\circ}\text{C}$, near-single-phase NiTi wires are created and the Kirkendall porosity increases, leading to a variety of pore/channel structures: (i) for 25 μm Ni wires where diffusion distances and times are short, a high volume fraction of micropores is created near the final NiTi wire surface, with 1–2 larger pores near its core; (ii) for 50 μm Ni wires, a single, ~ 20 μm diameter pore is created near the NiTi wire center, transforming the wires into microtubes, and; (iii) for 100 μm Ni wires, a ~ 50 μm diameter irregular pore is formed near the NiTi wire center, along with an eccentric crescent-shaped pore of similar cross-section, resulting from interruption of a single diffusion path, due to the longer diffusion distances and times.

Keywords

Shape-memory alloys, Diffusion, Phase transformation, Powder metallurgy, Microstructure

1. Introduction

The shape-memory effect (SME) and superelastic effect (SE) exhibited by bulk NiTi alloys with near-equiatomic composition are useful in many applications such as stents, bone implants, mechanical actuators and elastocaloric cooling devices [[1], [2], [3], [4]]. Introducing open porosity in NiTi can enhance the material performance, e.g., for improved heat exchange *via* a higher surface area or for improved osseointegration in bone implants with low stiffness which reduces stress shielding [5,6]. To date, porous NiTi has been primarily fabricated using powder-metallurgy processes with placeholders, such as steel wires or tubes that are electrochemically dissolved [7,8], Mg ribbons which are evaporated [[9], [10], [11]], salts (NaCl [12] and NaF [13]) that are leached out, or an inert gas (Ar [5,14]) that is expanded at high temperatures to create the porous structure. However, because of the low diffusivity in the ordered NiTi lattice, NiTi sintering requires very long times, even at temperatures near the melting point of NiTi (1310 $^{\circ}\text{C}$), increasing the risks of contamination or composition drift *via* Ti oxidation [15]. Alternatively, NiTi structures with fully controlled porosity or channels can be created *via* selective laser melting (SLM) of pre-alloyed NiTi powders [[15], [16], [17], [18]], but this method faces challenges such as high oxidation sensitivity of liquid NiTi exacerbated by the high surface/volume ratio of the melt pool, the need for pre-alloyed NiTi powders with tight composition control, and, upon solidification, development of undesirable coarse grain size, grain texture, surface roughness and residual porosity. Recently, we demonstrated a different additive approach to create NiTi with pores in structures, such as wires, where one dimension is small (below ~ 200 μm): we used a gas-phase alloying technique to deposit Ti onto Ni wires and then homogenized the wire to achieve a uniform NiTi composition, while taking advantage of the Kirkendall effect during interdiffusion to form a central channel, resulting in a microtube [19,20]. We previously used this method to create microtubes in the Ni—Cr—Al system, by homogenizing Ni—Cr microwires on which Al had been deposited [21].

The Kirkendall effect [22] describes the generation of microscopic voids near the interface of two atomic species with different diffusivities; the imbalance in diffusivities results in a net flux of atoms, leaving excess vacancies on the side of the faster diffusing species, which then coalesce into a large number of microvoids. Typically, the Kirkendall effect is considered detrimental to material properties due to the weakening associated with these voids [23]. For the Ni—Ti system, Bastin and Rieck [24] showed that Ni diffuses faster than Ti in most of the relevant phases between 650 and 940 $^{\circ}\text{C}$. However, the presence of other intermetallic phases – i.e., Ni_3Ti , NiTi_2 , and Ni_4Ti_3 – complicates the kinetics of interdiffusion; thus, NiTi synthesis *via* interdiffusion demands tight compositional control [25]. Pack cementation, a simple and scalable chemical vapor deposition (CVD) process, is

capable of such fine compositional control (e.g. ± 0.1 at.% for equiatomic NiTi with repeatable SME or SE properties) [26]. Moreover, the use of pack cementation for porous metallic foams [[27], [28], [29]] and woven wire structures [[30], [31], [32]] is well established.

We have recently demonstrated, for the first time, the formation of NiTi microtubes upon homogenization of Ti-coated Ni wires where interdiffusion creates Kirkendall voids which coalesce to create a tube with a central channel [19,20]. This exploratory study was conducted on a single Ni wire diameter (50 μm) and focused on 3D tomographic reconstruction to quantify the pore formation during homogenization, with limited exploration of phase and pore evolution during the prior Ti deposition. Here, we further investigate the formation of NiTi microtubes by considering a range of Ni wire sizes (25, 50, and 100 μm) and by quantifying the evolution of various Ni—Ti phases and the Kirkendall pores associated with the Ni—Ti interdiffusion occurring during Ti deposition as well as subsequent homogenization.

2. Experimental procedures

Pure Ni wires (99.99% purity) were purchased from Alfa Aesar in 25, 50, and 100 μm diameter sizes. Wires were cut into 3–4 cm segments and batches of up to 12 wires were embedded in a powder pack, which consisted of 67 wt.% TiC as an inert filler (Atlantic Equipment Engineers, -325 mesh, 99.9% purity), 30 wt.% Ti as the source material (Alfa Aesar, -325 mesh, 99.5% purity), and 3 wt.% NH_4Cl as the activator (Alfa Aesar, 100 μm , 99.5% purity). Previously, it was noted that TiC powders were occasionally embedded in the wires during titanization where they remained during homogenization [19]. As this could have a detrimental effect on the mechanical properties of the wires, the as-received TiC powders were sieved using a -325 mesh (44 μm opening) sieve and the finer particles, which are more likely to be embedded, were discarded. After mechanically mixing for 30 min, ~ 20 g of pack was poured in an alumina crucible, which was then covered with a thin TiC powder layer, followed by the Ni wire segments and another thin TiC powder layer. The Ni wires were sandwiched between two thin TiC powder layers to allow easy removal of the wires after titanization, since the pack particles can partially sinter during the process. Finally, ~ 20 g of pack was added on top, so that the wires were at the center of the powder pack.

The crucible, covered with an alumina lid, was then placed in the water-cooled end of a pre-heated tube furnace which was flushed for 15 min with Ar. The crucible was then pushed into the hot zone of the furnace in ~ 60 s, fast enough to prevent premature activation of the pack before it reaches the hot zone of the furnace but slow enough to prevent cracking of the crucible due to thermal shock. All titanization procedures were conducted at 925 $^\circ\text{C}$ in accordance with previous work [19]. This is below the lowest eutectic temperature in the Ni—Ti binary system (942 $^\circ\text{C}$), but still corresponds to a wide composition range for the near-equiatomic NiTi. Following titanization, the crucible was pulled back to the water-cooled end of the furnace and allowed to cool for several hours under continuous Ar flow. The wires were then removed from the pack and cleaned ultrasonically in acetone for 15 min.

The Ti-coated Ni wires were homogenized to create a uniform NiTi phase and the Kirkendall pores. First, the titanized wires were encapsulated in evacuated quartz capillaries (0.6 and 0.8 mm inside and outside diameters, respectively) with magnesium strips to create a Mg atmosphere, thus preventing reactions with residual oxygen in the capillaries. All homogenization treatments were carried out at the same temperature as the pack cementation, 925 $^\circ\text{C}$, though times were varied to observe phase evolution mechanisms and to identify the homogenization duration needed to eliminate composition gradients for each wire size. After homogenization, the capsules were air-cooled and the wires were ultrasonically cleaned in acetone.

Microstructural characterization was performed on wire cross-sections, using both optical microscopy (OM, Nikon MA-200) and scanning electron microscopy (SEM, Hitachi S3400N-II) with energy dispersive X-ray

spectroscopy (EDS) for compositional analysis. The wires were mounted in epoxy, ground and polished down to 0.05 μm finish. When necessary, images were analyzed using ImageJ open source digital image analysis software [33]. Multiple cross-sections from multiple wires were observed, and three representative micrographs for each processing condition were analyzed for phase and pore area fractions.

3. Results and discussion

3.1. Pack-titanization

3.1.1. 25 μm diameter Ni wires

The goal of the titanization step is to add Ti to the surface of the wires such that the average wire composition is as close as possible to equiatomic NiTi. For 50 μm diameter Ni wires, it was previously established that this optimal titanization time is 2 h at 925 $^{\circ}\text{C}$ [19]. Thus, for 25 μm diameter Ni wires, the optimal time is expected to be shorter by a factor of 4 (i.e., 0.5 h), given that diffusion distance scales with the square root of time (neglecting geometrical effects associated with cylindrical geometry). Thus, titanization for the 25 μm diameter Ni wires was carried out for 0.25, 0.5, and 1 h. Representative cross-sections of these titanized wires are presented in Fig. 1. Fig. 1a shows four distinct shells, which are identified *via* EDS, from outermost layer to the core, as NiTi₂, NiTi, Ni₃Ti, and Ni. Extensive, interconnected micro-porosity is present in the outermost, ~ 10 μm thick NiTi₂ shell, which can be explained by an uneven Ti deposition and/or local Kirkendall pore formation upon NiTi₂ formation as Ti is deposited from the gas phase (no Ti layer is observed). Furthermore, a crescent-shaped pore was observed between the Ni₃Ti and NiTi layers, as shown in Fig. 1a with an arrow. In other cross-sections (not shown here), smaller crescent-shaped pores or even smaller disconnected pores were observed. This suggests that the crescent-shaped pore observed in Fig. 1a is not continuous along the axis of the wire and is still developing in different parts of the wire. After 0.5 h titanization, two separate pores are visible in the cross-section displayed in Fig. 1b. An irregular shaped pore (labeled I) is nearly at the halfway point between the center and the surface of the wire, and a crescent-shaped pore (labeled II) is near the center, which once again appears at the Ni₃Ti/NiTi interface. Pore II likely formed early on, similar to the crescent-shaped pore observed after 0.25 h in Fig. 1a and was left behind as the NiTi/Ni₃Ti interface moved towards the center. It is possible that it was larger in size, but partially sintered during interdiffusion. The near-surface micropores present after 0.25 h (Fig. 1a) have disappeared in Fig. 1b, and a smooth NiTi₂ outer shell surrounds the fiber. However, in a small number of cross-sections imaged, the micropores were still present. The disappearance of the micropores may have occurred *via* sintering and/or *via* filling with Ti deposited from the gas phase. EDS confirmed that the average wire composition is close to 50 at.% Ti. Finally, after 1 h titanization (Fig. 1c), the overall Ti content is > 50 at.%, as expected, and the NiTi₂ outer shell has thickened considerably, mostly at the expense of the NiTi inner shell which itself has consumed the Ni core and the thin Ni₃Ti layer. No significant change is observed in the crescent shape or size of the inner pore/channel.

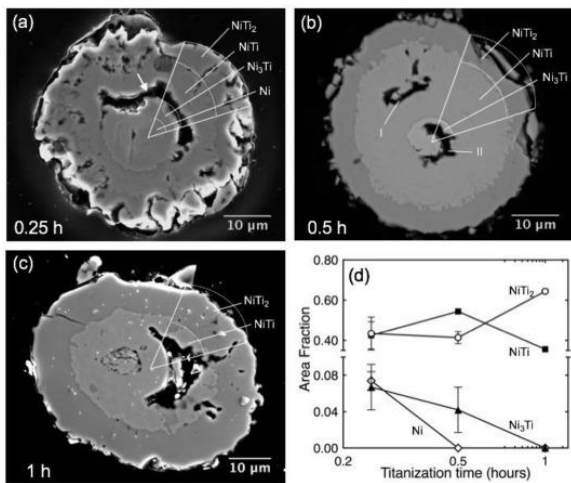


Fig. 1. Backscatter electron micrographs showing radial cross-sections of 25 μm diameter Ni wires titanized at 925 °C for (a) 0.25 h, (b) 0.5 h, (c) 1 h; thin white lines illustrate boundaries between various phases; (d) semi-logarithmic plot of phase fraction as a function of titanization time. Error bars smaller than the data markers are not displayed.

Using three images per condition and EDS scans of each, the area fractions of the phases were calculated and they are plotted in Fig. 1d for each titanization time. While phases were measured as area fractions based on the polished circular cross-sections, 3D tomographic reconstructions in previous work [19] give a strong case for cylindrical symmetry, so that area fraction can be considered to be equal to volume fraction. Fig. 1d shows that the Ni core shrinks as Ti is added to the wire and diffuses inwards to form the other phases, in particular NiTi and NiTi₂ which grow over the first 0.5 h. After 1 h, however, the NiTi region shrinks, as it is consumed by the advancing NiTi₂ outer shell.

3.1.2. 50 μm diameter Ni wires

Expanding upon the experiments reported in Ref. [19] where a single titanization time of 2 h was used, 50 μm diameter Ni wires were titanized here for 0.25, 0.5, 1, 2, and 4 h at 925 °C, with representative cross-sections shown in Fig. 2a–e. After 0.25 h, the wires exhibit a large Ni core, surrounded by a thin Ni₃Ti shell (~3 μm wide), a thick NiTi shell (~7 μm wide) and a thin NiTi₂ outer shell (~2 μm wide), as confirmed *via* EDS. This is the same shell configuration seen in Fig. 1 for 25 μm Ni wires titanized for the same time. However, less near-surface porosity is visible, but this difference is not significant as other cross-sections displayed more or less near-surface porosity. As titanization time increases, the outer NiTi₂ shell grows radially outwards and the NiTi shell grows radially inwards at the expense of the Ni₃Ti inner shell and the Ni core (Fig. 2b–e). The fine pores present in the outer NiTi₂ shell after 0.25 h (Fig. 2a) disappeared after 0.5 h (Fig. 2b), though they are still present in some cross-sections, consistent with the behavior of the 25 μm diameter wires over the same time range (Fig. 1a and b), possibly due to sintering or filling with Ti. An initial uneven coating may also be responsible, as seen in other systems where pack cementation was used for metal deposition [34]. The rough outer surface of the wires observed in Fig. 2b–e, where small fragments of the NiTi₂ outer shell were fractured, but are embedded in the mounting medium, is due to damage during metallographic preparation.

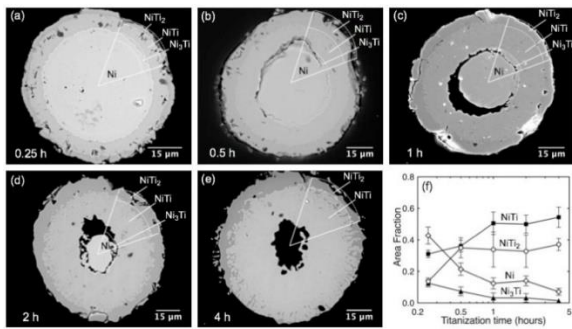


Fig. 2. Backscatter electron micrographs showing radial cross-sections of 50 μm diameter Ni wires titanized at 925 °C for (a) 0.25 h, (b) 0.5 h, (c) 1 h, (d) 2 h, and (e) 4 h; thin white lines illustrate boundaries between various phases; (f) semi-logarithmic plot of phase fraction as a function of titanization time. Error bars smaller than the data markers are not displayed.

A crack-like circumferential pore was observed as early as 0.5 h (Fig. 2b), which grew into crescent-shaped pores in later stages. At 1 h, different cross-sections showed no pores, crack-like pores, or crescent shaped pores, likely due to small variations in starting coating thicknesses at different cross-sections. Fig. 2d shows, after 2 h of titanization, the core-shell structure most clearly with a configuration of concentric cylindrical shells. A crescent-shaped pore at the center of the wire, which seems to be the dominant pore formed at 2 h, is separating the Ni core from the inner Ni₃Ti layer. The core-shell structure observed here is very similar to the one reported in a previous study, which used the same processing conditions [19]: 5, 15 and 7 μm layer thicknesses were observed for the Ni₃Ti, NiTi and NiTi₂ shell thicknesses, respectively, as compared to 5, 20 and 9 μm in Fig. 2d. Small variations in layer thicknesses (also reported in Ref. [19]) and in presence/absence of pores (none are reported in Ref. [19]) from one cross-section to the other are expected. Upon a final doubling of titanization time from 2 to 4 h (Fig. 2e), the wires mostly consist of single-phase NiTi with a shell of NiTi₂ remaining close to the wire outer surface, suggesting over-titanization with Ti/Ni > 1 (atomic ratio).

The phase evolution in the 50 μm diameter Ni wires is plotted in Fig. 2f. Like the 25 μm diameter wires, the Ni core shrinks quickly as Ti is added to the surface and diffuses inward to form the other phases. The Ni₃Ti layer slowly disappears as the pores separate it from the Ni core and cuts off the Ni supply, whereas Ti atoms diffusing from the surface transform Ni₃Ti into NiTi. The as-received Ni wires used here are in the annealed condition, hence, a coarse grain structure is expected in the Ni wire and remaining Ni core, though the newly created Ni—Ti intermetallic phases could have finer grains. As a result, volume diffusion, particularly in the early stages, should be the dominant mechanism during deposition and interdiffusion.

3.1.3. 100 μm diameter Ni wires

Given that, for 50 μm diameter Ni wires, the optimal titanization time to achieve equiatomic compositions is 2 h at 925 °C [19], a four-fold increase in titanization time to 8 h is expected for the 100 μm diameter Ni wires. To gain insight into the early evolution of phases and the nature of internal void formation, Ni wires were subjected to titanization for times of 0.25, 0.5, 1, 2, 4, and 8 h (15, 30, 60, 120, 240, and 480 min) and compositions were determined *via* EDS. For the longer times, pack exhaustion may occur, *i.e.*, Ti deposition stops due to loss of halides to the partially open system *via* the flowing cover gas. Therefore, at titanization times of 2, 4, and 6 h, wires were removed and placed into a fresh pack and the process continued for a 2 h interval.

Representative cross-sections for Ni wires titanized for various times are shown in Fig. 3. As expected, as Ti is added to the wire and diffuses inwards, the Ni core shrinks while the NiTi₂, NiTi, Ni₃Ti shells (also seen in the smaller diameter wires) grow (Fig. 3a–c). After 0.25 h (Fig. 3a), fine porosity is present in the NiTi₂ outer shell and to a lesser extent after 0.5 h (Fig. 3b), consistent with the behavior of the two finer wires (Fig. 1, Fig. 2a-b).

The surface microporosity completely disappears after 1 h. Up to 2 h titanization, the microstructure evolution closely resembles the 50 μm wires in Fig. 2, with the growth of the outer shells and a decrease in the diameter of the Ni core. At 2 h, however, a thin, crack-like pore is visible between the NiTi and Ni₃Ti shells, spanning an arc of $\sim 90^\circ$. This circumferential crack-like pore, created from the coalescence of numerous Kirkendall pores, interrupts the radial diffusion paths for Ni and Ti and thus slows homogenization kinetics, as further discussed in Section 3.2.3. A similar crack-like pore is also present in some cross-sections of the 50 μm diameter wires (Fig. 2b). After 4 h titanization (following a pack change after 2 h), some cross-sections show arc-shaped crack-like pores between the NiTi and Ni₃Ti shells (Fig. 3e), whereas others display crescent-shaped pores indicating that the crack-like pores formed after 2 h are growing. Finally, Fig. 3f after 8 h of titanization (following a pack change after 2, 4 and 6 h) shows (i) a crack-like pore (labeled I) observed at the same depth as the pore seen after 4 h (Fig. 3e), but spanning nearly half the circumference, and (ii) a new, near-360° crack-like pore, close to the wire center and surrounding the unreacted Ni core (labeled II). The new pore II is probably formed by the same Kirkendall mechanism as the earlier, pore I, occurring after the diffusion path has been interrupted by the formation of the latter pores.

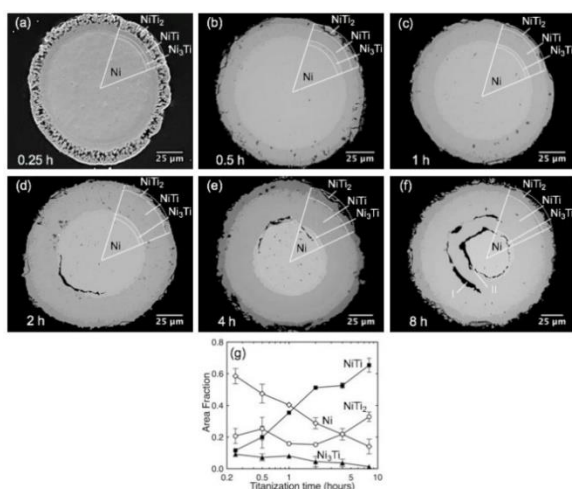


Fig. 3. Backscatter electron micrographs showing radial cross-sections of 100 μm diameter Ni wires titanized at 925 $^\circ\text{C}$ for (a) 0.25, (b) 0.5 h, (c) 1 h, (d) 2 h, (e) 4 h, and (f) 8 h, with pack changes every 2 h; thin white lines illustrate boundaries between various phases; (g) semi-logarithmic plot of phase fraction as a function of titanization time. Error bars smaller than the data markers are not displayed.

Fig. 3g shows a plot for phase evolution during titanization of the 100 μm Ni wires. Similar to the 50 μm Ni wires, there is a steady decrease in Ni phase fraction as the core is consumed by the growth of Ti-rich phases. The NiTi fraction steadily increases during the first 2 h. The pack changes after 2, 4 and 6 h ensure that more Ti is added, as evidenced by the growth of both NiTi and NiTi₂ phases.

3.1.4. Titanization evaluation

The phase evolution described so far clearly shows that interdiffusion and Kirkendall porosity occur extensively during the titanization step under conditions of continuing Ti deposition at the wire surface. Even for the longest titanization times for each wire diameter, no more than 65 vol.% NiTi is achieved. Using the stoichiometric composition of the phases - equiatomic for the NiTi shell and pure Ni for the Ni core (a good approximation since average Ti concentration in Ni is found to be very small) - the average concentration of Ti in the wires is calculated, as shown in Fig. 4, at each titanization step based on the measured phase fractions (given in Fig. 1, Fig. 2, Fig. 3g). Optimal titanization times, for which near-equiatomic Ni/Ti concentration, is reached, are the starting points for the homogenization steps. Reaching the near-equiatomic composition is important because both superelastic and shape-memory properties are observed around this range. For the 25 μm Ni wires, 0.5 h is

sufficient to achieve ~50 at.% of Ti in the wire. For 50 μm diameter Ni wires, the equiatomic composition is reliably reached after 2 h, in good agreement with previous research [19]. Some 50 μm wires achieve equiatomic NiTi average composition after only 1 h, but error bars are large for this time; the modest Ti gain between 1 and 2 h may be an indicator of pack exhaustion. Finally, for 100 μm Ni wires, Fig. 4 shows that little Ti gain is achieved after 2 h if the pack is not changed. With pack changes every 2 h, by contrast, near equiatomic NiTi average composition is achieved after 8 h titanization.

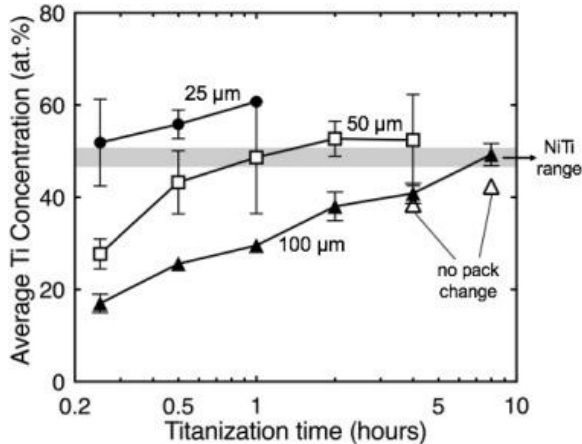


Fig. 4. Semi-logarithmic plot of average Ti concentration in Ni wire vs. titanization time for the three wire diameter sizes, including cases where the pack was changed or not changed for the 100 μm diameter wire. NiTi concentration range at 925 $^{\circ}\text{C}$ is marked. Error bars smaller than the data markers are not displayed.

3.2. Homogenization after titanization

3.2.1. 25 μm diameter Ni wires

The 25 μm diameter Ni wires which had been titanized for 0.5 h exhibited a diameter of ~45 μm after Ti deposition (here and below, the wires are described based on their original diameter before titanization). Five different homogenization times at 925 $^{\circ}\text{C}$ were chosen: 0.25, 0.5, 1, 2, and 4 h. Each homogenized wire was divided into at least three sections, then mounted, polished, and observed *via* SEM. Fig. 5a–e displays a representative cross-section for each homogenization time, from which phase fractions were measured.

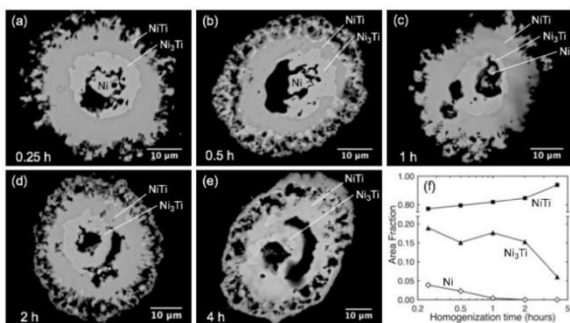


Fig. 5. Backscatter electron micrographs showing radial cross-sections of 25 μm diameter Ni wires homogenized at 925 $^{\circ}\text{C}$ for (a) 0.25 h, (b) 0.5 h, (c) 1 h, (d) 2 h and (e) 4 h. Wires were previously titanized at 925 $^{\circ}\text{C}$ for 0.5 h. (f) Semi-logarithmic plot of phase fraction as a function of homogenization time. Error bars smaller than the data markers are not displayed.

Starting from the cross-section shown in Fig. 1b after titanization - showing a small Ni core and two wide NiTi and NiTi₂ shells, together with one crescent and one irregular pore - the homogenization process leads to formation of extensive near-surface porosity, likely formed *via* the Kirkendall effect at one or more phase interfaces (Fig. 5a–e). At both 0.25 and 0.5 h (Fig. 5a and b), a small Ni core is present together with Ni₃Ti and

NiTi shells. For longer homogenization times (Fig. 5c and d), the Ni core disappears, as it is consumed by Ni₃Ti which becomes the core, and the wire achieves 94 vol.% NiTi by 2 h, with trace amounts of Ni_xTi_ySi_z near the surface. The latter phase was probably created by reaction of the wires with SiO₂ from the capsules and/or with gaseous SiO created by partial reduction of SiO₂ with Mg vapor. The evolution of phase fraction is shown in Fig. 5f (where pores are not considered during measurements). The short diffusion distances and times resulted in wires with extensive micropores (1–5 μm in size); near the surface, pore areal fraction is as high as 6%. Both circular and crescent-shaped pores, fewer in number but larger in size, are observed near the center of the wires. The crescent-shaped pores were observed during titanization (Fig. 1a–c) and early evidence for the formation of a central pore is seen in Fig. 1c. If they can be fabricated with repeatable and controlled composition, these porous NiTi microwires may be attractive for applications where high surface area is desirable, e.g., for rapid heat transfer.

3.2.2. 50 μm diameter Ni wires

The 50 μm Ni wires used for homogenization were titanized for 2 h and exhibit well-defined, smooth shells of ~50 vol.% NiTi, ~35 vol.% NiTi₂, ~2 vol.% Ni₃Ti, and ~13 vol.% Ni core (Fig. 2d and f). The addition of Ti added ~30 μm to the overall diameter, for a total ~80 μm. Based on previous work [19], four homogenization times were studied at 925 °C: 2, 4, 8, and 16 h. Fig. 6a–d shows representative cross-sections for each homogenization time.

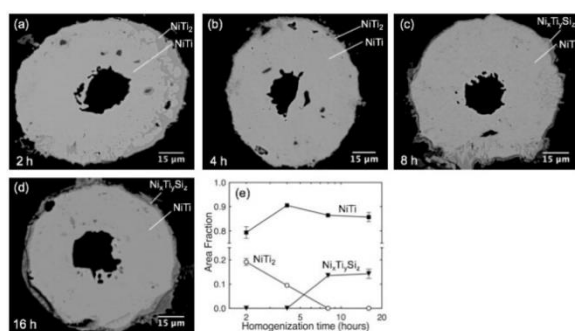


Fig. 6. Backscatter electron micrographs showing radial cross-sections of 50 μm diameter Ni wires homogenized at 925 °C for (a) 2 h, (b) 4 h, (c) 8 h, and (d) 16 h. Wires were previously titanized at 925 °C for 2 h. (e) Semi-logarithmic plot of phase fraction as a function of homogenization time. Error bars smaller than the data markers are not displayed.

After 2 h homogenization (Fig. 6a), the wire is 80 vol.% NiTi and 20 vol.% NiTi₂ is present as a partial outer shell; the wire displays a distinct central pore/channel with near-circular cross-section. The fraction of NiTi further increases to ~90 vol.% after 4 h, with a concomitant decrease to 10 vol.% NiTi₂. For longer times of 8 and 16 h (Fig. 6c and d), this Ti-rich phase disappears indicating complete homogenization, but the Ni_xTi_ySi_z silicide phase forms at the wire surface; this phase can be avoided in future experiments by coating the quartz capsule with a non-reactive material such as boron nitride or by using non-quartz capsules. Nevertheless, as reported in our previous study [20], a NiTi wire containing significant amounts of silicide exhibited shape memory and superelastic properties after homogenization for 16 h. Additionally, Fig. 6b shows remaining TiC particles which were embedded in the wire during Ti deposition, and which can cause stress concentrations and detwinning of the martensitic phase, leading to lowered stiffness [35]. Fig. 6e shows the evolution of the various phases. In all cases, the central cavity is ~20 μm in diameter, and does not sinter, up to the longest homogenization time of 16 h. It shows a serrated surface indicative of merger of smaller Kirkendall pores, and is similar in shape, location and morphology to the cavity present in the wire titanized for 4 h (Fig. 2e). Results presented here are in good agreement with those discussed in our previous work [19]. In both studies, a central, near-circular pore with a diameter of ~20 μm is developed at ~2 h and stayed stable up to the longest homogenization time of 16 h.

3.2.3. 100 μm diameter Ni wires

For the 100 μm Ni wires, homogenization times of 4, 8, 16, 24, and 32 h were used to investigate different stages of pore development. Representative SEM micrographs of cross-sections are shown in Fig. 7a–e for the above five homogenization times at 925 $^{\circ}\text{C}$, using Ni wires which had been titanized for 8 h, and whose diameter had grown in the process from 100 to 165 μm .

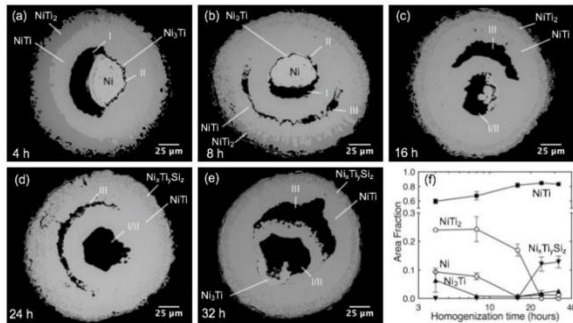


Fig. 7. Backscatter electron micrographs showing radial cross-sections of 100 μm diameter Ni wires homogenized at 925 $^{\circ}\text{C}$ for (a) 4 h, (b) 8 h, (c) 16 h (d) 24 h, and (e) 32 h. Wires were previously titanized at 925 $^{\circ}\text{C}$ for 8 h, with pack changes every 2 h. (f) semi-logarithmic plot of phase fraction as a function of homogenization time. Error bars smaller than the data markers are not displayed.

The 100 μm Ni diameter wire sections display an evolution different from those of the 50 μm Ni wires. A double-pore configuration is dominant at all homogenization times, which is consistent with the pore structure in the original 8h-titanized wire with two circumferential, crack-like pores - one closer to the wire center and the other closer to the surface (labeled I and II in Fig. 3f) – whose formation is discussed in Section 3.1.3. Fig. 7a, after 4 h homogenization, shows a wide crescent-shape cavity (marked I in Fig. 7a), covering an arc of $\sim 180^{\circ}$ on the left side of the wire. This pore interrupts the radial diffusion path between a NiTi shell and a partial NiTi₂ surface shell on one side, and the Ni inner core on the other side of the pore. On the other (right-side) half of the wire, a thin crescent pore (marked II in Fig. 7a) is present, which is connected at its ends with the wider pore (I); together, the two pores separate completely the inner Ni core from the outer shells. Its smaller width (2–3 μm) and its location closer to the wire center indicate that pore II formed later than pore I which is consistent with the absence of NiTi₂ outer shell on the right half of the wire, indicative of an uninterrupted diffusion path. The interruption of the radial diffusion path by pores I and II, which together fully surround the Ni core, does not completely preclude homogenization, since longitudinal mass transfer may still occur *via* solid bridges interrupting these pores (which are likely extending into the length of the wires as channels), outside the two-dimensional cross-sections shown in Fig. 7a. Such bridges were imaged in Ref. [19] which provided tomographic reconstructions of 50 μm wires homogenized for 2 h at 925 $^{\circ}\text{C}$; however, diffusion distances are lengthened through such intermittent bridges and diffusional cross-sections are reduced which slow the homogenization kinetics of the wires.

Fig. 7b, after 8 h homogenization, shows the same combination of a Ni core surrounded by a wide crescent pore/channel (I) and thin opposite crescent pore/channel (II) closer to the wire surface, with a partial NiTi₂ shell on the wire surface closest to the wide pore (I). A third crescent pore (III) has formed between the first pore (I) and the surface, consistent with interdiffusion between the NiTi₂ and NiTi shells. After 16 h homogenization, Fig. 7c, the NiTi wire displays a central oblong pore (I/II) with approximate cross-section dimensions of 25 \times 50 μm , probably created from the merger and further growth of pores I and II, together with a further decrease of the Ni core. The crescent pore (III) has widened and coarsened (and has a slightly larger area than pore I/II), consistent with its draining of nearby Kirkendall pores and vacancies. Cross-sections after 24 and 32 h homogenization, Fig. 7d and e, show modest growth of the near-central circular pore (I/II) and the eccentric

crescent pore (III) (their radial orientation vary, as expected since the cross-sections are from distinct wires), as the Ni core is slowly being consumed, and the NiTi₂ outer shell is being replaced by the Ni_xTi_ySi_z silicide phase due to Si contamination. Small amounts of the Ni₃Ti outer shell remain. Our previous study [20] showed that Ni₃Ti does not affect the superelastic properties of microtubes because NiTi can accommodate that phase. However, Ni₃Ti is brittle and may have hindered strain recovery somewhat as the maximum strain recoverable was below expected [36].

Fig. 7f summarizes the evolution of the phase volume fractions, confirming the growth of the NiTi phase during homogenization. Similar to the 50 μm Ni wires (Fig. 6e), towards later times (24 and 32 h), Si contamination from the quartz capsule creates the Ni_xTi_ySi_z phase which prevents achieving pure NiTi. The values in Fig. 7f are averages of three cross-sections taken within the same wire at different depths. Within the same wire, there may be the development of somewhat different microstructures at different locations, especially with respect to the location of the central cavity, which forms a complex channel structure in 3D [19]. These wires are three-dimensional, and longitudinal diffusion cannot be observed by taking 2D cross-sections. Such measurements would require the use of X-ray tomography as was carried out in previous studies [19,21].

3.3. Summary of phase and pore evolution

The results presented above show the effect of initial wire size, or diffusion distance, on the evolution of various phases and Kirkendall pores in the titanized Ni wires. Fig. 8 schematically illustrates, for all three wires at the same magnification, the four stages of processing: as-received drawn Ni wire, early-stage titanized Ni wire, final-stage titanized Ni wire with 50 at.% Ti, and homogenized NiTi wire. This figure illustrates and summarizes the effect of initial Ni wire size on the subsequent phase evolution, and pore/channel morphology, size and locations.

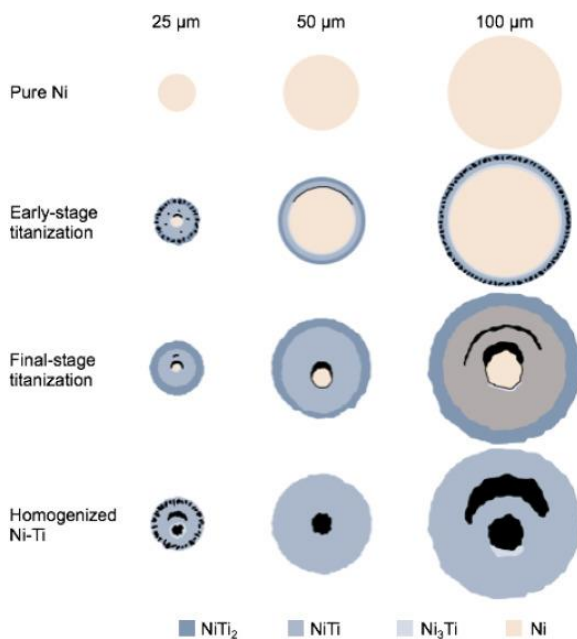


Fig. 8. Schematic representation of the evolution of phases and Kirkendall pores in titanized Ni wires with original diameters of 25, 50, and 100 μm, at different stages of processing.

At the early stages of titanization, some wires show small pores in the NiTi₂ layer, located very close to the wire surface. This was particularly visible in the 25 and 100 μm wires. At the later stages of titanization, these pores either sintered or are filled with Ti during continued titanization. Another distinct feature is the double-pore structure observed in most wires at the late-stage titanization step. This is due to leaving behind a large pore (or

a group of smaller pores) that formed early in the process, while the phase interfaces move inwards and create another large pore at the center of the wire. This double-pore configuration is visible in all wire sizes but becomes increasingly common as the wire size increases. For 100 μm Ni wires, double-pores are visible in every cross-section.

The most apparent effect of the diffusion distance is seen in the homogenized structure. As the wires are homogenized to obtain single phase NiTi, we see (i) high volume fraction of surface porosity in 25 μm wires as pores preferentially annihilate at the wire surface given shorter diffusion distance; (ii) a single central pore in 50 μm wires, which effectively drain all vacancies and smaller pores which coalesce into a single cavity; and (iii) a double-pore structure in 100 μm wires, where pores formed during titanization do not sinter or merge with other pores and continue their growth upon homogenization.

4. Conclusions

Building on our recent previous research performed on Ni wires with 50 μm diameter [19,20], we show here that porous wires with near-equiatomic NiTi composition can be fabricated by Kirkendall pore formation during titanization and homogenization at 925 $^{\circ}\text{C}$ of both thicker and thinner Ni wires (25 and 100 μm diameters). The evolution of phases and pores during titanization and homogenization indicates a strong size effect. Several conclusions can be drawn from this work:

1. Ni wires with 25 μm diameter:
 - (a) Titanization for 0.5 h results in the formation of a core/multiple-shell structure consisting of NiTi₂, NiTi, Ni₃Ti, and Ni phases, with a larger crescent-shaped pore forming close to the center of the wire.
 - (b) Subsequent homogenization for 1–4 h achieves homogenous NiTi wires with many Kirkendall micropores near the surface and 1–2 near-cylindrical larger central Kirkendall pores.
2. Ni wires with 50 μm diameter:
 - (a) Titanization for 2 h results in a similar core/multiple-shell structure with the same phases seen in 25 μm wires. A few central micropores form at the NiTi/Ni₃Ti interface.
 - (b) Subsequent homogenization for 2–8 h results in a NiTi wire with a single, larger, ~ 20 μm diameter central pore.
3. Ni wires with 100 μm diameter:
 - (a) Titanization for 8 h forms the same phases observed in the other wires, but with two crack-like circumferential pores; one surrounding the unreacted Ni core and the other between the surface and the first pore.
 - (b) Subsequent 16–32 h homogenization results in NiTi wires exhibiting a dual circular and crescent-shape pore structure, spanning 40–80 μm in size, which evolved from the above-mentioned pores.

Acknowledgements

This work was funded by the National Science Foundation under award number DMR-16-11308. This work made use of the EPIC facility (NUANCE Center-Northwestern University), which has received support from the MRSEC program (NSF DMR-1720139) at the Materials Research Center, and the Nanoscale Science and Engineering Center (EEC-0118025/003), both programs of the National Science Foundation; the State of Illinois; and Northwestern University. This work also made use of the MatCI Facility which receives support from the MRSEC Program (NSF DMR-1720139) of the Materials Research Center at Northwestern University.

References

- [1] L.S. Castleman, S.M. Motzkin, F.P. Alicandri, V.L. Bonawit, A.A. Johnson, J. Biomed. Mater. Res., 10 (1976), pp. 695-731
- [2] Q. Chen, G.A. Thouas, Mater. Sci. Eng. R Rep., 87 (2015), pp. 1-57
- [3] H. Huilong, S. Emrah, S. Drew, H. Naila Al, Q. Suxin, O. Ryan, C. Jun, T. Ichiro, J. Phys. Appl. Phys., 50 (2017), p. 404001
- [4] J. Frenzel, G. Eggeler, E. Quandt, S. Seelecke, M. Kohl, MRS Bull., 43 (2018), pp. 280-284
- [5] C. Greiner, S.M. Oppenheimer, D.C. Dunand, Acta Biomater., 1 (2005), pp. 705-716
- [6] A. Bansiddhi, T.D. Sargeant, S.I. Stupp, D.C. Dunand, Acta Biomater., 4 (2008), pp. 773-782
- [7] C. Bewerse, A.A. Emery, L.C. Brinson, D.C. Dunand, Mater. Sci. Eng. A, 634 (2015), pp. 153-160
- [8] C. Bewerse, L.C. Brinson, D.C. Dunand, J. Mater. Process. Technol., 214 (2014), pp. 1895-1899
- [9] C. Bewerse, L.C. Brinson, D.C. Dunand, Acta Mater., 115 (2016), pp. 83-93
- [10] T. Aydogmus, S. Bor, J. Mech. Behav. Biomed. Mater., 15 (2012), pp. 59-69
- [11] T. Aydogmus, S. Bor, J. Alloy. Comp., 478 (2009), pp. 705-710
- [12] A. Bansiddhi, D.C. Dunand, Acta Biomater., 4 (2008), pp. 1996-2007
- [13] A. Bansiddhi, D.C. Dunand, Intermetallics, 15 (2007), pp. 1612-1622
- [14] S.M. Oppenheimer, D.C. Dunand, Mater. Sci. Eng. A, 523 (2009), pp. 70-76
- [15] M.H. Elahinia, M. Hashemi, M. Tabesh, S.B. Bhaduri, Prog. Mater. Sci., 57 (2012), pp. 911-946
- [16] S. Dadbakhsh, M. Speirs, J.-P. Kruth, J. Van Humbeeck, CIRP Ann. - Manuf. Technol., 64 (2015), pp. 209-212
- [17] M. Elahinia, N.S. Moghaddam, M.T. Andani, A. Amerinatanzi, B.A. Bimber, R.F. Hamilton, Prog. Mater. Sci., 83 (2016), pp. 630-663
- [18] C. Haberland, M. Elahinia, J.M. Walker, H. Meier, J. Frenzel, Smart Mater. Struct., 23 (2014)
- [19] A.E. Paz y Puente, D.C. Dunand, Intermetallics, 92 (2018), pp. 42-48
- [20] A.E. Paz y Puente, D.C. Dunand, Acta Mater., 156 (2018), pp. 1-10
- [21] A.E. Paz y Puente, D. Erdeniz, J.L. Fife, D.C. Dunand, Acta Mater., 103 (2016), pp. 534-546
- [22] A.D. Smigelskas, E.O. Kirkendall, Trans. Am. Inst. Min. Metall. Eng., 171 (1947), pp. 130-142
- [23] K.J. Zeng, R. Stierman, T.C. Chiu, D. Edwards, K. Ano, K.N. Tu, J. Appl. Phys., 97 (2005)
- [24] G.F. Bastin, G.D. Rieck, Metall. Trans., 5 (1974), pp. 1827-1831
- [25] A. International, **ASM Handbook: Alloy Phase Diagrams**, ASM, Materials Park, OH (1992)
- [26] R. Mevrel, C. Duret, R. Pichoir, Mater. Sci. Technol., 2 (1986), pp. 201-206
- [27] H. Choe, D.C. Dunand, Acta Mater., 52 (2004), pp. 1283-1295
- [28] D.C. Dunand, A.M. Hodge, C. Schuh, Mater. Sci. Technol., 18 (2002), pp. 326-332
- [29] A.M. Hodge, D.C. Dunand, Intermetallics, 9 (2001), pp. 581-589
- [30] D. Erdeniz, A.J. Levinson, K.W. Sharp, D.J. Rowenhorst, R.W. Fonda, D.C. Dunand, Metall. Mater. Trans., 46 (2014), pp. 426-438
- [31] D. Erdeniz, K.W. Sharp, D.C. Dunand, Scripta Mater., 108 (2015), pp. 60-63
- [32] C. Wang, D.C. Dunand, Metall. Mater. Trans., 46 (2015), pp. 2249-2254
- [33] C.A. Schneider, W.S. Rasband, K.W. Eliceiri, Nat. Methods, 9 (2012), pp. 671-675
- [34] D. Erdeniz, D.C. Dunand, Intermetallics, 50 (2014), pp. 43-53
- [35] A.J. Neurohr, D.C. Dunand, Acta Mater., 59 (2011), pp. 4616-4630
- [36] K. Otsuka, X. Ren, Prog. Mater. Sci., 50 (2005), pp. 511-678

¹Currently at: SiNode Systems, Chicago, IL, 60616, USA.

²Currently at: Department of Mechanical Engineering, Marquette University, Milwaukee, WI, 53233, USA.